



The Effect of Drying of Glycerol-Plasticized Starch upon Its Dielectric Relaxation Dynamics and Charge Transport

Stavros X. Drakopoulos^{1,4} · Zdenko Špitalský² · Hamed Peidayesh² · László Lendvai³

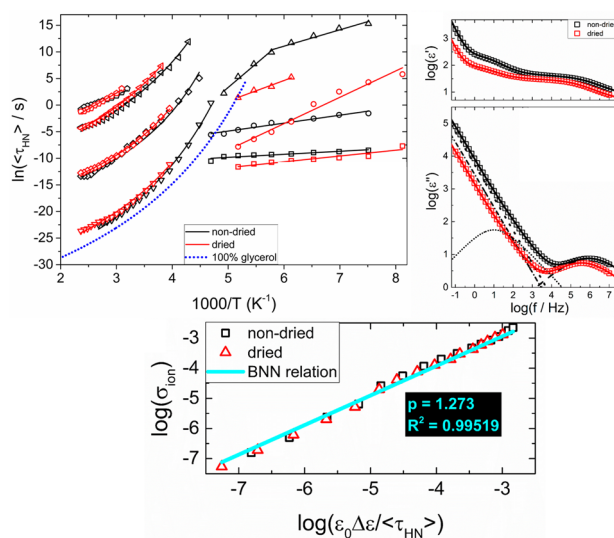
Accepted: 7 June 2023 / Published online: 30 June 2023

© The Author(s), under exclusive licence to Springer Science+Business Media, LLC, part of Springer Nature 2023

Abstract

Carbohydrate polymers are promising materials for an eco-friendly future due to their biodegradability and abundance in nature. However, due to their molecular characteristics and hydrophilicity, are often complicated to be investigated via spectroscopic methods. Thermoplastic starch plasticized by glycerol was prepared through melt processing conditions using twin screw extruder. Here we show how the presence of water molecules affects the dielectric response and charge transport dynamics over broad frequency (10^{-1} to 10^7 Hz) and temperature (-140 to 150 °C) ranges. Overall, 7 dielectric processes were observed and differentiation between electronic and ionic conductivities was achieved. Two segmental relaxation processes were observed for each sample, ascribed to the starch-rich and glycerol-rich phases. Although the timescales of the two segmental relaxations were found different, both arise from the same temperature, giving thus an alternative explanation on what is reported in the literature. The origin of the σ -relaxation was attributed to hydrogen ions and was found to be proportional to the ionic conductivity according to the Barton, Nakajima and Namikawa relation. The presence of water molecules was found to enhance the ionic conductivity, indicating that water contributes charge carriers when compared to the dried sample.

Graphical Abstract



Keywords Broadband dielectric spectroscopy · Carbohydrates · Relaxation dynamics · Charge transport · Polymer physics · Thermoplastic starch

Introduction

As the depletion of fossil fuels progresses through the 21st century, petroleum-based products like synthetic polymers need to be recycled or replaced by equivalent eco-friendly alternatives [1, 2]. One of the alternatives is sustainable polymers that originate from renewable resources and the agricultural industry [3, 4]. The fact that plant-based polymers are often abundant in nature, while most of them are also biodegradable and biocompatible makes them good candidate materials for various applications ranging from biomedicine and tissue engineering to packaging [5–11]. A major class of plant-based polymers is polysaccharides and a significant representative material is starch [12]. Native starch is a semi-crystalline polymer, which occurs in the form of isolatable granules in the size range of 2–100 μm . Starch granules are composed of two polymers, namely amylose and amylopectin, both being built up of 1,4 α Dglucopyranosyl repeating units [13]. While amylose is a linear polysaccharide, amylopectin has a highly branched molecular structure. The crystalline structure of native starch can be mostly attributed to the amylopectin chains that are arranged into a double helical structure [14]. Due to a large number of hydrogen bonds between its macromolecules, the processing of starch is rather difficult, since they hamper the mobility of the molecules greatly [15]. Therefore, unlike conventional thermoplastics, starch undergoes degradation instead of melting when exposed to heat. Under the appropriate processing conditions, starch can be transformed from a semicrystalline biopolymer to a gelatinized material [4, 16, 17]. This new state is achieved in the simultaneous presence of plasticizers, mechanical shear stresses and heat that gradually destroy the initial crystalline structure and create a new kind of material, which is widely known as plasticized starch, or destructed starch. Under the above-described circumstances, molecular motion gets initiated, which allows the chains to slide past one another. The applied plasticizers can come in various forms, including water, polyols (e.g. glycerol, sorbitol, mannitol) and compounds that possess amino groups (e.g. urea, formamide) [18]. Regarding the processing techniques, various methods can be applied that are also commonly used in the plastic industry, such as extrusion, blowing, casting, compression moulding or injection moulding [19–21]. According to the literature, shortly after the melt processing a new single-helical crystalline structure gets formed, which is attributed to the fast recrystallization of amylose [22, 23]. This material with this new structure is generally referred to as thermoplastic starch (TPS), which is also dominated by hydrogen bonds [24, 25].

During the design of short-lived applications like packaging, catering, or biomedicine, it is only logical to avoid employing long-lasting polymers for sustainability

purposes. Agro-resources such as polysaccharides like starch find application in the food, textile, paper, and adhesives industry [23]. After partial or complete gelatinization, TPS foams can be used in shock absorbable and isothermal packaging that can be extended to more applications. However, due to its intensive moisture sensitivity TPS is mostly used, when blended with other green polymers [26] or reinforced with fillers [4, 16, 17]. This way, it can become a suitable material for various products in the field of agriculture, sport, hygiene and food packaging or storage [27].

Polysaccharides, like starch and TPS, are complicated polymers from a molecular spectroscopy point of view because of the complexity of glucose, the various polymeric structures that arise from it, water content and interfaces between the constituents [28]. Thus, the interpretation of the resulting spectra is often ambiguous, depending on the technique [29]. One of the most prominent techniques in molecular spectroscopy and materials physics is Broadband Dielectric Spectroscopy (BDS). BDS is the go-to technique to examine the dielectric relaxation processes, charge transport, and molecular transitions in insulating or semiconducting materials and their composites in broad temperature and frequency ranges [30–33].

In the present paper, the presence of adsorbed water is discussed in terms of the dielectric properties of TPS plasticized with glycerol. Our target is to understand better how thermoplastic starch behaves under the application of an external ac electric field and draw some parallel with ionically conductive polymers. The dielectric spectra were tested in broad frequency and temperature ranges, revealed seven dielectric processes. From the observed processes, three are attributed to secondary relaxations of starch and two are segmental relaxations ascribed to the glycerol-rich and starch-rich phases. At temperatures above 0 °C, the dielectric response was dominated by the presence of migrated hydrogen ions (σ -relaxation) and electrode polarization. Finally, the charge transport dynamics of both electronic and ionic conductivities are presented. The presence of adsorbed water was observed to enhance the ionic conductivity indicating that water contributes charge carriers.

Experimental Section

Materials

A commercially available native maize starch, Meritena 100 (Brenntag, Slovakia) was used as the basic polymer. The plasticizer for starch was glycerol of 99% purity (Central-Chem, Ltd.). Prior to any processing, the starch powder was stored in a WGLL-125 BE type drying chamber (Huanghua Faithful Instrument) at 80 °C overnight to eliminate its

inherent moisture content. Subsequently, it was manually premixed with glycerol at the ratio of 2:1 (starch:glycerol) and the resulting dry mixture was fed into an LTE 20–44 co-rotating twin screw extruder (Labtech Engineering). The ratio of the components was based on our previous study [34]. The temperature of the extruder barrel from feeder to die end was the following: 85, 90, 95, 100, 100, 100, 110, 110, 120, 120 °C. The screw diameter was 20 mm, while the l/d of the screw was 44 and the rotation speed was set to 75 rpm.

Sample Preparation

After melt compounding, the samples were compression moulded at 130 °C using an SRA-100 type heated press (Fontijne Presses). Initially, the moulds were closed for two minutes without any applied pressure and then they were closed for two minutes under 2.65 MPa. The non-dried sample was used as is, whilst the dried sample was conditioned overnight at 50 °C under vacuum. The humidity content was determined via mass measurements prior and after drying and was found to be $4.65 \pm 0.07\%$ w/w. Cylindrical samples resulted in thicknesses of 359 μm and 329 μm for the non-dried and dried samples respectively.

Broadband Dielectric Spectroscopy

BDS was performed in a temperature-controlled chamber using an Alpha analyser provided by Novocontrol Technologies, Germany. The voltage amplitude V_{rms} of the applied field was kept constant at 1 V, at the frequency range of 10^{-1} to 10^7 Hz. The temperature was controlled via the Quattro system (with ± 0.1 °C accuracy) and the dielectric test cell used was the BDS-1200, parallel-plate capacitor, with two gold-plated electrodes system. To assure good contact, gold electrodes were plated into the samples with a diameter of 20 mm. The isothermal scans were measured in the temperature range of -140 to 150 °C, in steps of 10 °C. Noise in the dielectric spectra of the dried sample was observed at temperatures between -70 and -30 °C and as such these temperatures were not analysed via the Havriliak-Negami function model to avoid inconsistencies in the discussion.

Results and Discussion

Dielectric Response

The dielectric response of the samples under study as a function of temperature is presented in Fig. 1 employing the dielectric permittivity and the electric modulus formalisms. The complex relative dielectric permittivity $\epsilon^*(\omega)$ is defined below:

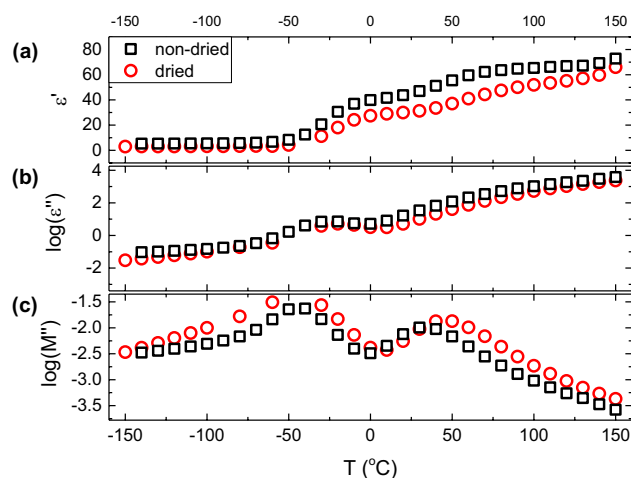


Fig. 1 Comparative representation of **a** real part and **b** imaginary part of dielectric permittivity and **c** imaginary part of electric modulus as a function of temperature at 10^4 Hz for both samples

$$\epsilon^*(\omega) = \epsilon'(\omega) - i\epsilon''(\omega) \quad (1)$$

where $\epsilon'(\omega)$ and $\epsilon''(\omega)$ are the real and imaginary parts of relative dielectric permittivity respectively. Although the dielectric permittivity is the most commonly employed formalism, the use of different dielectric formalisms like electric modulus, ac conductivity and impedance is very beneficial towards a complete analysis [35, 36]. Thus, the complex electric modulus $M^*(\omega)$ is connected to the complex dielectric permittivity as seen in Eq. (2):

$$\begin{aligned} M^*(\omega) &= \frac{1}{\epsilon^*(\omega)} = \frac{\epsilon'(\omega)}{[\epsilon'(\omega)]^2 + [\epsilon''(\omega)]^2} \\ &+ i \frac{\epsilon''(\omega)}{[\epsilon'(\omega)]^2 + [\epsilon''(\omega)]^2} \\ &= M'(\omega) + iM''(\omega) \end{aligned} \quad (2)$$

where $M'(\omega)$ and $M''(\omega)$ are the real and imaginary parts of electric modulus respectively.

Figure 1a shows the real part of dielectric permittivity that increases with increasing temperature, indicating that the dipoles' orientation is a thermally assisted process [37]. The ϵ' values below -50 °C appear to be constant with two consecutive steps arising at -50 °C and 30 °C respectively. The two dielectric processes correspond to the dynamic glass-to-rubber transition processes (α -relaxation) of the glycerol-rich and starch-rich areas respectively [38]. It is evident that upon drying, the ϵ' values decrease throughout the whole temperature range. Since the presence of water prior to drying is due to adsorbed molecules in hydrophilic starch, the decrease in ϵ' values indicates that water contributes to polarization. When water is employed in larger quantities during the

manufacturing of the samples to serve as a plasticizer, its evaporation has been observed to have the opposite effect (increase ϵ' values) since the polarizability of polar groups is facilitated [37, 39].

According to the imaginary parts of dielectric permittivity and electric modulus (Fig. 1b and c) at the temperature range below -50 °C, the indication of secondary dielectric processes exists, as expected [29], in the form of a shoulder although at this frequency (10^4 Hz), peaks are not clearly observed. Above -50 °C, M'' shows two clear peaks corresponding to the α -relaxations for the glycerol and TPS rich

phases, slightly shifted towards lower temperatures compared to ϵ'' . The use of electric modulus shifts dielectric phenomena to a higher frequency which translates to lower temperatures in isochronal conditions through the time-temperature superposition. The presence of secondary relaxation processes is firmly discussed in Figs. 2 and 3.

Havriliak-Negami Fittings

To further investigate the dielectric spectra and discern between the contributions of the various processes, the

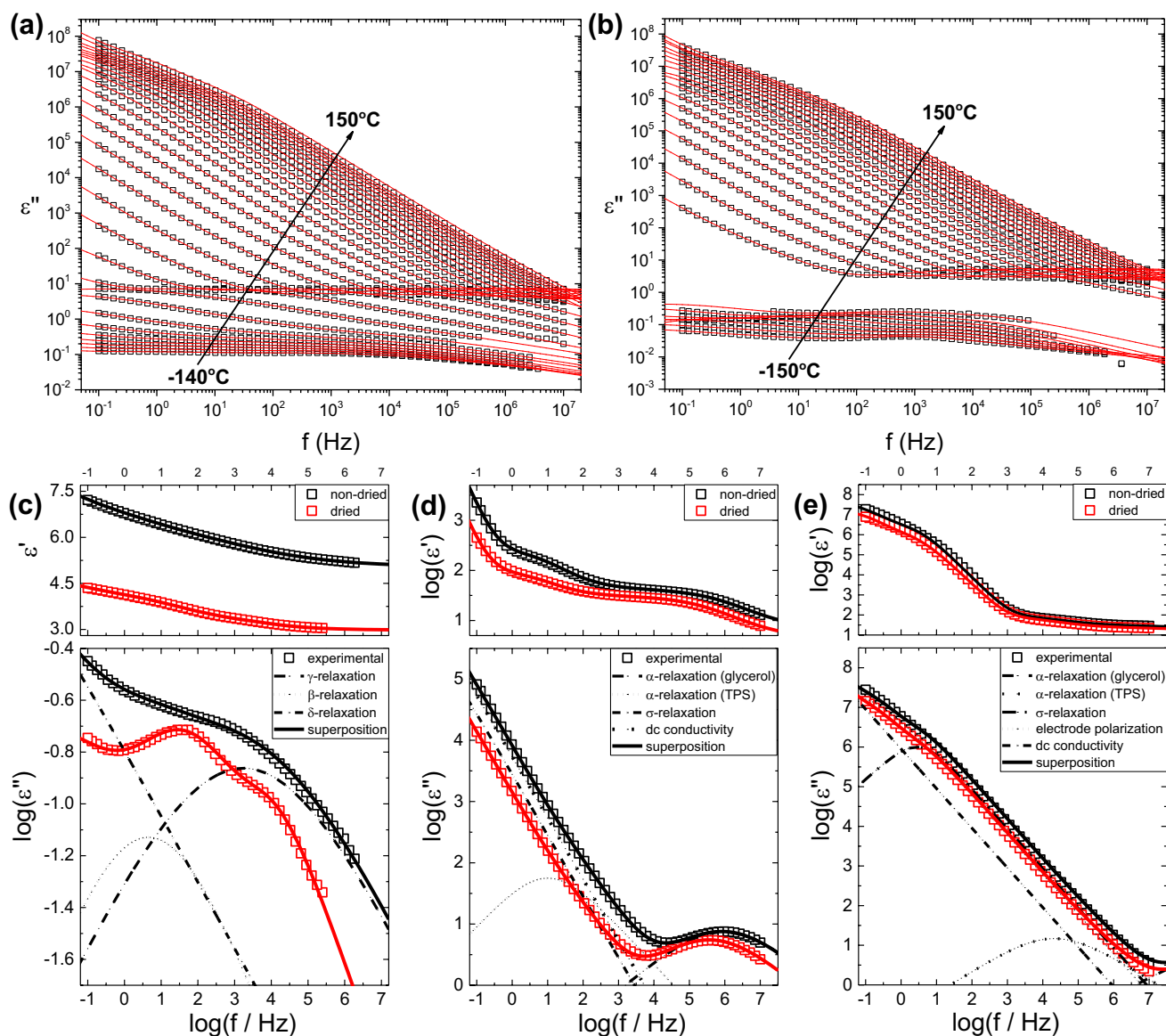


Fig. 2 The imaginary part of dielectric permittivity as a function of frequency at varying temperature including the experimental (symbols) and Havriliak-Negami fittings (lines) for: **a** non-dried and **b** dried TPS samples. The lines correspond to the superposition of Havriliak-Negami curves and the conductivity term. The correspond-

ing fittings for the real and imaginary parts of dielectric permittivity at **c** -100 °C, **d** 0 °C, and **e** 100 °C are presented in detail with the deconvoluted Havriliak-Negami and conductivity fittings being shown only for the non-dried sample

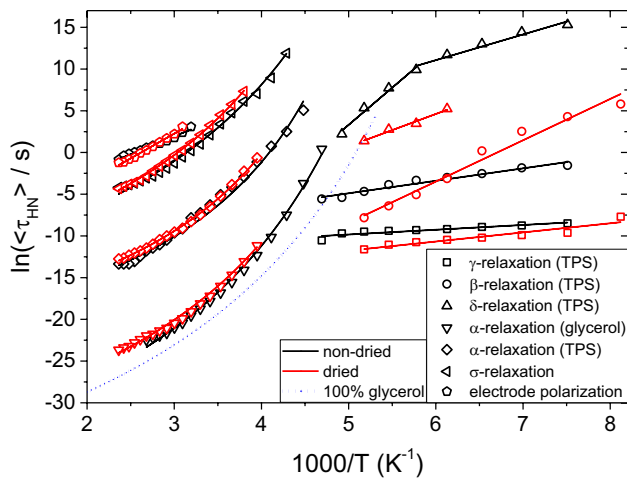


Fig. 3 Relaxation map with the Havriliak-Negami relaxation times of the dielectric processes throughout the entire temperature range observed for both samples. The blue dotted line corresponds to the re-created α -relaxation dynamics of pure glycerol based on the VFT parameters provided by Puzenko et al. [58] for comparison reasons. The Arrhenius and VFT fittings parameters are presented in Table 1 below. The error of the obtained isothermal $\langle \tau_{HN} \rangle$ values is expected to be 5% or less

semi-empirical Havriliak-Negami (HN) function model was employed. Here, the HN function model is utilized in its generalized complex permittivity form for N relaxation processes and conductivity contribution:

$$\epsilon_{HN}^*(\omega, T) = \epsilon_\infty + \sum_{i=1}^N \left[\frac{\Delta\epsilon}{[1 + (i\omega\tau_{HN})^m]^n} \right] + \frac{\sigma_{dc}(T)}{i\epsilon_0\omega^s} \tag{3}$$

$$\langle \tau_{HN} \rangle = \frac{1}{\omega_{max}} \left[\frac{\sin\left(\frac{m\pi}{2+2n}\right)}{\sin\left(\frac{mn\pi}{2+2n}\right)} \right]^{\frac{1}{m}} \tag{4}$$

where ω is the angular frequency, $\langle \tau_{HN} \rangle$ corresponds to the average HN relaxation time, $\Delta\epsilon$ is the dielectric relaxation strength where $\Delta\epsilon = \epsilon_s - \epsilon_\infty$ with ϵ_s and ϵ_∞ being the static and infinite frequency permittivity values respectively ($\epsilon_s = \lim_{\omega \rightarrow 0} \epsilon'$ and $\epsilon_\infty = \lim_{\omega \rightarrow \infty} \epsilon'$) and ϵ_0 is the free space permittivity (8.854×10^{-12} F/m). Shape parameters m and n correspond to the symmetrical and asymmetrical distribution of relaxation times, respectively with $0 < m \leq 1$ and $0 < mn \leq 1$; for $m = n = 1$ Eq. (3) reduces to the Debye model for a single relaxation time [40]. The electronic conductivity σ_e is assumed to result in pure losses (no induced polarization) and in Eq. (3) is presented as σ_{dc} . The values of σ_{dc} were determined isothermally by employing Eq. (3). In the present systems, parameter s was observed to be equal to unity ($s = 1$) indicating pure Ohmic charge mechanism for

σ_{dc} . More information on the parameter s can be found elsewhere [30, 41]. The complete frequency-dependent Havriliak-Negami fittings against the experimental data at all temperatures are shown at Fig. 2a and b for the non-dried and the dried samples respectively. The individual fittings at -100°C , 0°C and 100°C are shown at Fig. 2c, d and e with the deconvoluted contributions shown for the non-dried sample.

In total, 7 dielectric processes were observed, namely γ -, β -, δ - relaxations, the α -relaxations of the glycerol-rich and the starch-rich phases, the σ -relaxation and finally the electrode polarization (from low to high temperature). Contrary to most polymers, in carbohydrates the δ -relaxation is observed at higher temperatures than the γ - and β -relaxations [29]. The physical origin and the dielectric characteristics of each are going to be discussed in detail below. It should be noted here that no β_{wet} -relaxation was observed in the case of the non-dried sample. The presence of water molecules for the non-dried sample corresponds to adsorbed water only, which is not enough to give rise to β_{wet} -relaxation. Due to the absence of fillers and excess water, no contribution of interfacial polarization in the overall dielectric response was observed either. Generally, interfacial polarization (also known as MWS-IP) appears in heterogeneous materials, where the individual phases are characterized by different electrical properties (dielectric constant and/or electrical conductivity values) [35]. In plain thermoplastic starch, interfacial polarization has not been observed in the past although it was visible in the imaginary part of electric modulus for TPS-based composites [37, 39]. However, the presence of interfacial polarization cannot be eliminated given the heterogeneous nature of TPS, although the high values of σ -relaxation and electrode polarization can potentially mask it. Still, no indication of it was observed at the imaginary part of electric modulus either as with other cases of similar materials [37, 39].

At the temperature range below -60°C in total three dielectric processes were observed, namely the γ -, β -, and δ - relaxations and are attributed exclusively to starch [29] since no secondary relaxations are known for glycerol [42, 43]. Since the gelatinization of starch in the presence of glycerol results in the melting of starch crystallites, the relaxation dynamics are expected to vary compared to untreated, pristine starch [44, 45]. The presence of the γ -, and β -relaxation processes in carbohydrate polymers are due to the orientation of hydroxyl groups and local main chain dynamics, respectively. The origin of δ -relaxation has been attributed to end groups and as such is particularly visible in branched macromolecules. For the dried sample, both the γ - and the β -relaxation processes were observed to be broad and asymmetrical. The Cole-Cole parameter was observed to be $m = 0.672 \pm 0.032$ and 0.597 ± 0.159 for the two processes respectively, while the Davidson-Cole parameter

was found to be $n = 0.699 \pm 0.146$ and 0.502 ± 0.286 . The δ -relaxation was found to be symmetrical ($n = 1$) but broad with $m = 0.374 \pm 0.040$. The secondary relaxation processes of the non-dried sample were found to require different Havriliak-Negami shape parameters with both the γ - and the β -relaxation processes being symmetrically broad ($n = 1$) with shape parameters $m = 0.279 \pm 0.012$ and 0.441 ± 0.067 respectively. The δ -relaxation for the non-dried sample was described with $m = 0.388 \pm 0.008$ and $n = 0.750 \pm 0.123$, where m and n are the average values over temperature obtained at isothermal conditions and the errors correspond to the standard deviation.

As mentioned previously, the two α -relaxation processes correspond to the dynamic glass-to-rubber transition processes of the glycerol-rich and starch-rich areas respectively [38, 46, 47]. The dynamic glass-to-rubber transition process (also known as the segmental relaxation) corresponds to the cooperative relaxation of the amorphous segments of a polymer chain whilst approaching the glass transition temperature (from high to low temperatures) [48–50]. Via the Havriliak-Negami equation, we observed that the two α -relaxation processes for both samples are broadly symmetrical ($n = 1$). For the dried sample, the Cole-Cole shape parameter values were observed to be $m = 0.511 \pm 0.020$ and 0.602 ± 0.027 for the α -relaxations of glycerol and starch respectively. The non-dried sample exhibited very similar values yielding $m = 0.488 \pm 0.053$ and 0.591 ± 0.037 .

The σ -relaxation was observed at temperatures after the T_g of glycerol and corresponds to ion hopping that occurs in most polysaccharides [51]. For pure polysaccharides, it has been proposed by Einfeldt et al., that sufficient residue of hydroxyl groups is responsible for the migration of the hydrogen ions [51]. Indeed, in our study we observe the σ -relaxation to be even more intense (higher $\Delta\epsilon$ values) than reported for pristine carbohydrates, due to the presence of glycerol that contributes additional hydroxyl groups. The migration of ions produces polarization in its surrounding environment (contributes to the ϵ' values) and thus is described by an HN fit. Interestingly, the HN shape parameters of the σ -relaxation are somewhat unusual ($n > 1$ but always $mn \leq 1$ so the model stands both physically and mathematically) that result in a low frequency asymmetry. This unusual case of the HN function model could be the reason why fitting the Debye function model ($m = n = 1$) often fails to accurately describe similar materials like polyelectrolytes [52, 53]. The Havriliak-Negami shape parameters to describe the σ -relaxation were observed to be $m = 0.692 \pm 0.036$ and $n = 1.447 \pm 0.072$ for the dried and $m = 0.766 \pm 0.067$ and $n = 1.315 \pm 0.121$ for the non-dried. The proportionality of the σ -relaxation with the ionic conductivity is going to be discussed later at the “Charge Transport” section of the manuscript through the Barton, Nakajima and Namikawa (BNN) relation.

Finally, the effect of electrode polarization is observed at high temperatures and low frequencies and is considered a parasitic effect as it often masks the dielectric response caused by the molecular orientation [30]. It is particularly observed in lossy dielectric materials and is due to the immobilization of charge carriers at the electrode/sample interface and thus produces large macroscopic dipoles [54, 55]. To model the contribution of the electrode polarization in both samples, we used similar Havriliak-Negami shape parameters as with the σ -relaxation where $mn = 1$. This corresponds to a Debye behaviour at the high-frequency side of the peak.

$$\langle \tau_{HN} \rangle = \tau_0 e^{\frac{DT_v}{T-T_v}} \quad (5)$$

$$\langle \tau_{HN} \rangle = \tau_0 e^{\frac{E_A}{k_B T}} \quad (6)$$

Relaxation Dynamics

The temperature dependence of the relaxation times of the observed dielectric processes are following either the Vogel-Fulcher-Tammann model or the Arrhenius law according to Eqs. (5) and (6) respectively:

where D and T_v are the fragility parameter and the Vogel temperature respectively, E_A is the activation energy of the dielectric process, and k_B is the Boltzmann constant (8.617×10^{-5} eV/K). In either case, τ_0 is a pre-exponential factor that corresponds to the relaxation time at infinite temperature, and T is the absolute temperature. The fitting parameters are presented in Table 1. Usually, the VFT equation (or alternatively the Williams-Landel-Ferry equation) describes the temperature dependence of the dynamic glass-to-rubber transition process [56]. A coupling between the temperature dependencies of ionic conductivity and dynamic glass-to-rubber transition process has been observed in ion-conducting polymers [57], and thus is no surprise that here the σ -conductivity also follows a VFT trend. Other dielectric processes including secondary relaxations most often obey the Arrhenius law which allows the calculation of their corresponding activation energy E_A . Here, all γ -, β -, and δ -relaxations as well as electrode polarization follow the Arrhenius law. Although the absence of a β_{wet} -relaxation in the non-dried sample is already discussed, it is interesting to observe that the relaxation time of the δ -relaxation upon drying is reduced by approximately two orders of magnitude. This reinforces the notion that the δ -relaxation transforms to the β_{wet} -relaxation with increasing water content [29].

In terms of relaxation dynamics, the effect of drying has been particularly profound in the low-temperature relaxations of TPS. In either case, the activation energy values of the γ - and the β -relaxation processes increase in the dried

Table 1 VFT and Arrhenius fitting parameters based on equations

Dielectric process	VFT fitting parameters					
	Non-dried			Dried		
	τ_0 (s)	D	T_v (K)	τ_0 (s)	D	T_v (K)
α -Relaxation (glycerol)	8.0×10^{-16}	20.41	134.0	7×10^{-15}	17.75	138.0
α -Relaxation (TPS)	1.2×10^{-9}	12.50	152.0	2×10^{-9}	12.30	154.5
σ -Relaxation	1.2×10^{-6}	18.49	135.2	1.65×10^{-6}	16.90	145.0
	Arrhenius fitting parameters					
	Non-dried		Dried			
	τ_0 (s)	E_A (eV)	τ_0 (s)	E_A (eV)		
γ -Relaxation	3.08×10^{-6}	0.049	3.30×10^{-8}	0.094		
β -Relaxation	4.28×10^{-6}	0.129	3.90×10^{-15}	0.426		
δ -Relaxation						
Low T	6.13×10^{-4}	0.265	8.52×10^{-9}	0.333		
High T	1.18×10^{-18}	0.769				
Electrode polarization	1.81×10^{-5}	0.369	1.83×10^{-7}	0.511		

The fittings have $R^2 > 0.85$

samples, indicating that the adsorbed water molecules assisted the relaxation of the corresponding dipoles. At the higher temperature range, the dominant dielectric process, namely the α -relaxations of the glycerol-rich and starch-rich phases respectively and the σ -relaxation do not appear to be significantly affected by the presence of water molecules. The relaxation dynamics of pure glycerol are also presented as re-created by the VFT fitting parameters provided by Puzenko et al. [58] to compare with that of the glycerol-rich phase in TPS. It is evident that the relaxation dynamics of the glycerol-rich phase within the starch matrix are described by higher average values of the $\langle \tau_{HN} \rangle$ by an order of magnitude compared to pure glycerol. We attribute the slowing of the dynamics to confinement effects that essentially reduce the mobility of glycerol's segmental relaxation [59]. This can be expressed also as an increase in the values of the Vogel temperature, T_v , which in the present study (Table 1) was observed to be higher by 15–18 K compared to that of pure glycerol [58].

Another interesting result originating from our analysis is that the α -relaxation process of the starch-rich phase appears to be present at temperatures lower than reported in the literature [38]. Indeed, it is significantly slower than that of the glycerol-rich phase, but it arises at comparable temperatures (-50 °C), as seen in the relaxation map (Fig. 3). When considering the time-temperature superposition (TTS) principle, their timescale difference explains the temperature discrepancy observed by other techniques like Dynamic Mechanical Analysis, when measured at isochronal conditions (one constant frequency) [26].

In Fig. 4, the dielectric strength values, $\Delta\epsilon$, as calculated by the HN fittings are presented for the six relaxation processes observed for TPS. Based on the $\Delta\epsilon$ values of the γ - and β -relaxation processes shown at 4a and 4b respectively, in the non-dried sample, the higher $\Delta\epsilon$ values indicate that water molecules participate in the orientation of hydroxyl groups (γ -relaxation) but hinder the local movements of the main chain (β -relaxation), as opposed to the dried sample. In Fig. 4e, the $\Delta\epsilon$ values of the starch-rich α -relaxation appear to be almost temperature-independent for the dried samples whilst the non-dried sample exhibits a significant reduction from 20 °C. At the 40–45 °C range is where water evaporation initiates due to the vapor pressure of free water as observed in similar samples [39], this explains the discrepancy between the two samples and also indicates that water molecules contribute to the α -relaxation of the starch-rich phase. At the vicinity of 70 °C and higher, the $\Delta\epsilon$ values between the non-dried and the dried samples are very similar showing that the water molecules responsible for the discrepancy at lower temperatures have probably evaporated.

Charge Transport

In the following part, the charge transport dynamics are going to be discussed separately for the electronic and ionic conductivities, σ_e and σ_{ion} respectively. The σ_e values were determined via Eq. (3) fittings and correspond to pure losses that contribute only to the imaginary part of dielectric permittivity following $\sigma_e/(\epsilon_0\omega)$. Apart from the electronic conductivity, under the influence of an externally applied electric field, the hopping of hydrogen ions is contributing

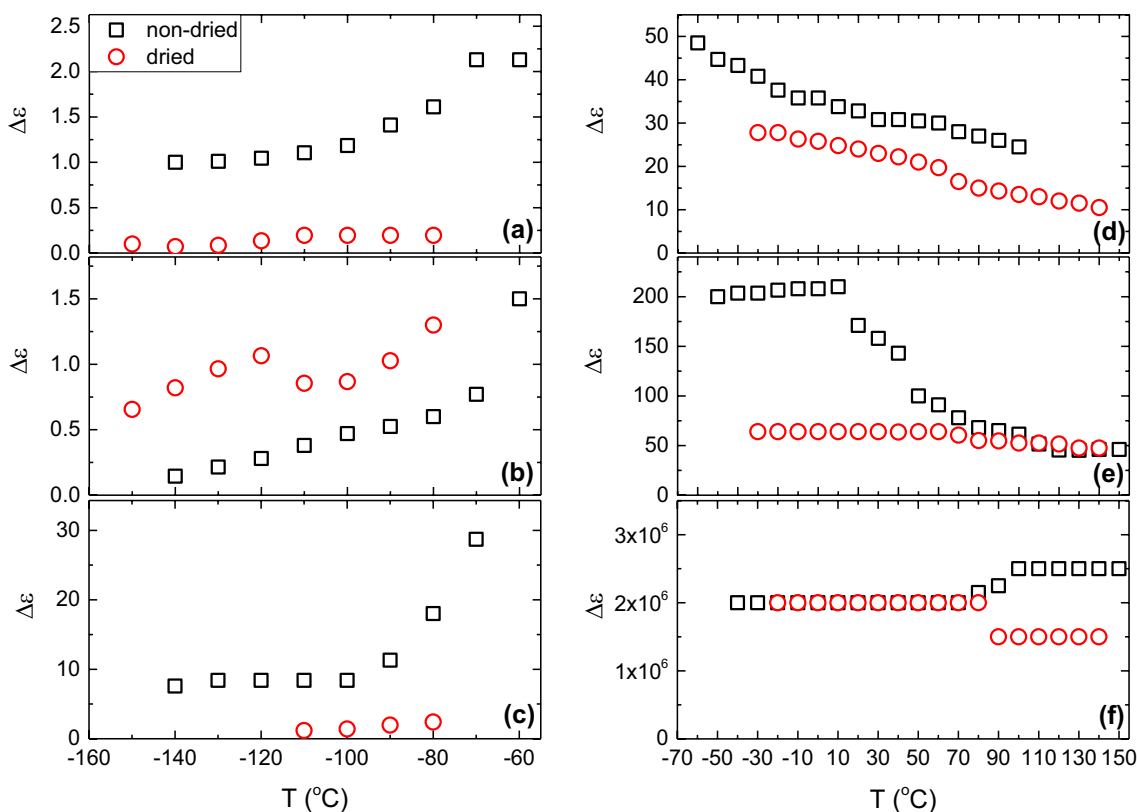


Fig. 4 The dielectric strength values as a function of temperature for both samples for: **a** γ -relaxation, **b** β -relaxation, **c** δ -relaxation, **d** α -relaxation (glycerol), **e** α -relaxation (TPS), and **f** σ -relaxation. The error of the obtained isothermal $\Delta\epsilon$ values is expected to be 5% or less

to the overall electrical conductivity of carbohydrate polymers [51]. To investigate ionic conductivity, we employed the complex ac conductivity σ_{ac}^* , which is defined as seen below:

$$\sigma_{ac}^* = i\epsilon_0\omega\epsilon^* \quad (7)$$

According to dielectric studies of solid-state polymer electrolytes, the ionic conductivity σ_{ion} can be calculated as the plateau value of σ'_{ac} where σ''_{ac} exhibits a minimum [60] under the assumption that the ionic conductivity is significantly higher than the electronic conductivity ($\sigma_{ion} \gg \sigma_e$). In the present work, particularly at low temperatures, the values between σ_{ion} and σ_e are comparable and hence to correctly estimate the isothermal values of σ_{ion} we first subtracted σ_e from σ'_{ac} . The temperature dependence of conductivity values exhibits either VFT or Arrhenius types respectively:

$$\sigma_{dc} = \sigma_0 e^{-\frac{DT_v}{T-T_v}} \quad (8)$$

$$\sigma_{dc} = \sigma_0 e^{-\frac{E_A}{k_B T}} \quad (9)$$

where σ_0 is the electrical conductivity at an infinite temperature with the rest of the parameters being already discussed previously at Eqs. (5) and (6). The VFT parameters and the activation energy values from the conductivity fittings are provided at Table 2 below.

As seen in Fig. 5a and b, both the dried and non-dried samples exhibit the typical ac conductivity behaviour of dielectric materials with ions hopping. This behaviour translates to an almost frequency-independent behaviour for σ'_{ac} at the frequency range that follows the peak observed at σ''_{ac} [60]. With increasing temperature, both σ'_{ac} and σ''_{ac} values increase indicating the thermally-assisted nature of charge transport in those materials [31]. This effect is highlighted in Fig. 5c where the temperature dependence of both electronic and ionic conductivities is presented for both materials under study.

According to Fig. 5c, the dynamics of both the ionic and electronic conductivities show a crossover at 40–45°C which is due to the gradual, in situ, evaporation of water that results in the change of slope for electrical conductivity [39]. Below that temperature, the ionic and the electronic conductivities follow the Arrhenius law described by relatively high activation energies ($E_A \sim 0.9$ eV) indicating a high energy barrier for charge transport. At

Fig. 5 Ac conductivity (real and imaginary parts) for the **a** non-dried and **b** dried TPS samples. **c** Charge transport dynamics for electronic and ionic conductivities as a function of reciprocal temperature. **d** Application of the BNN relation between the ionic conductivity and the dipolar characteristics of σ -relaxation

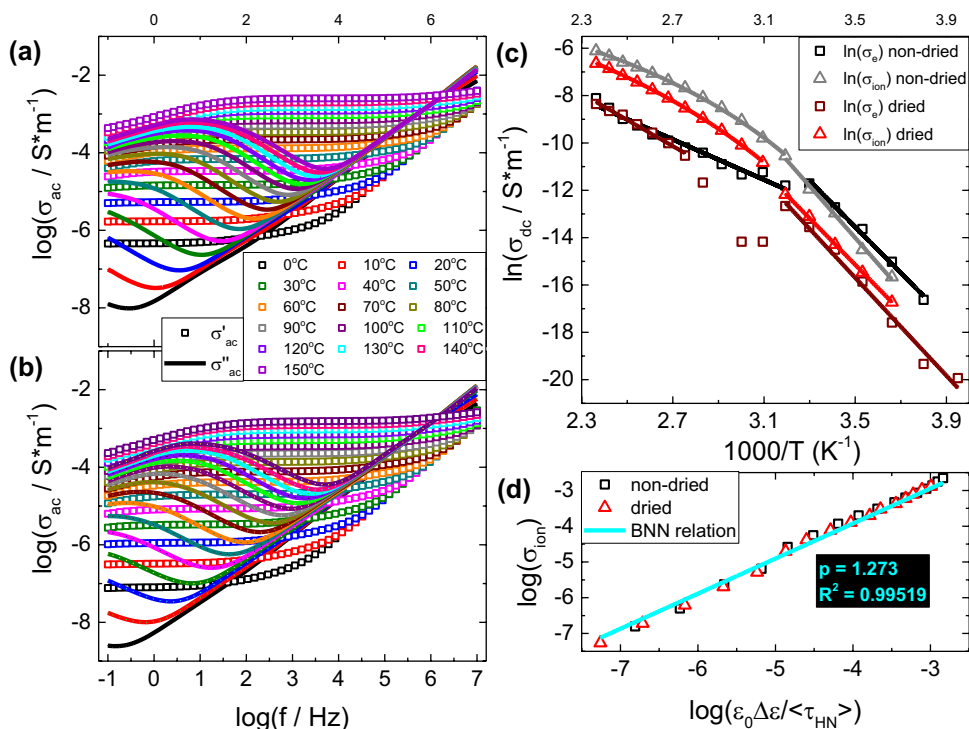


Table 2 VFT and Arrhenius fitting parameters for the temperature dependence of electronic and ionic conductivities

Regime	Arrhenius fitting parameters			
	Non-dried		Dried	
	E_A (eV)		E_A (eV)	
σ_e	Low T	0.838	0.891	
	High T	0.367	0.477	
σ_{ion}	Low T	0.941	0.845	
	VFT fitting parameters			
	Non-dried		Dried	
	D	T_v (K)	D	T_v (K)
σ_{ion}				
High T	4.012	211.89	5.894	198.09

The fittings have $R^2 > 0.97$

temperatures higher than the crossover, the activation energy of electronic transport reduces to $E_A \sim 0.4$ eV and the ionic conductivity follows a VFT temperature dependence. It is also evident that the non-dried TPS sample exhibits higher values for both σ_{ion} and σ_e throughout the whole temperature range. This observation lies in the fact that adsorbed water molecules are contributing charge carriers to conduction.

To examine the relationship between the σ -relaxation and the ionic conductivity we employ the Barton, Nakajima and Namikawa (BNN) relation [61] which describes the proportionality between the dipolar characteristics ($\Delta\epsilon$ and $\langle \tau_{HN} \rangle$) of σ -relaxation and σ_{ion} presented at Fig. 5d. The BNN relation follows Eq. (10) as seen below:

$$\sigma_{ion} = \frac{p\varepsilon_0\Delta\varepsilon}{\langle \tau_{HN} \rangle} \quad (10)$$

where $\Delta\varepsilon$ and $\langle \tau_{HN} \rangle$ are the relaxation dielectric strength and the average relaxation time of the σ -relaxation process, respectively, with p being a constant close to unity. The underlying physical explanation of the BNN relation lays its foundations on the random free-energy barrier model or symmetric hopping model [62, 63] and has found application in ionically conductive polymers [57, 64] among other ionic materials. In the present work, the applicability of the BNN relation is presented where a common fitting line can describe both the non-dried and dried samples with a calculated value of parameter p to be 1.273 and $R^2 = 0.99519$. The applicability of the BNN relation shows that indeed σ -relaxation is coupled to the corresponding ionic conductivity.

Conclusions

In summary, we investigated the dielectric response of thermoplastic starch prior to and after drying over a broad frequency and temperature range. Overall, we observed seven dielectric processes, five due to the samples' molecular characteristics, one due to ionic conductivity of hydrogen ions and one due to the parasitic effect of electrode polarization. The electronic conductivity was observed to follow a power law that contributes only at the imaginary part of dielectric permittivity. Between -150 and -60 °C, three secondary relaxations were observed namely γ -, β -, and δ -relaxations attributed to hydroxyl groups, local main chain dynamics, and end groups respectively. At the higher temperature range, two α -relaxations ascribed to the glycerol-rich and starch-rich phases respectively were found. The glycerol-rich α -relaxation was observed to be slowed down by an order of magnitude compared to pure glycerol, as a result of confinement effects from the surrounding starch matrix. Based on the Havriliak-Negami function analysis, we observed that the starch-rich α -relaxation arises from -50 °C similar to the glycerol-rich α -relaxation although the two processes are characterized by significantly different timescales. Based on the time-temperature superposition principle, their timescale difference explains why previous DMA studies have found the T_g of the starch-rich at the vicinity of 40 °C when performed in isochronal conditions (constant frequency). The presence of water molecules in the non-dried sample was found to enhance the ionic conductivity, indicating that water contributes charge carriers. Finally, the ionic conductivity was found proportional to the dielectric characteristics of the σ -relaxation according to the BNN relation. This shows that they share the same physical mechanism

attributed to the migration of hydrogen ions that produce polarization in the surrounding environment.

Acknowledgements The authors would like to thank professor Dr. Ivan Chodák (Slovak Academy of Sciences, Slovakia) for valuable discussions over TPS-based materials and for reading and providing with constructive comments about the manuscript prior to submission.

Author Contributions SXD: Conceptualization, Methodology, Formal analysis, Data curation, Writing—original draft, Writing—review & editing, Visualization, Supervision. ZŠ: Methodology, Validation, Investigation, Resources, Writing—review & editing. HP: Methodology, Validation, Investigation, Writing—review & editing. LL: Conceptualization, Methodology, Investigation, Writing—review & editing, Supervision, Project administration, Funding acquisition.

Funding H.P. would like to acknowledge financial help from The Slovak Grant Agency under the project number VEGA 2/0109/23.

Declarations

Conflict of interest There are no conflicts of interest to declare.

References

- Newell P (2019) Trasformismo or transformation? The global political economy of energy transitions. *Rev Int Polit Econ* 26:25–48. <https://doi.org/10.1080/09692290.2018.1511448>
- Krauss LM (2021) *Physics of climate change*. Apollo, New York
- Chung Y-L, Ansari S, Estevez L et al (2010) Preparation and properties of biodegradable starch–clay nanocomposites. *Carbohydr Polym* 79:391–396. <https://doi.org/10.1016/j.carbpol.2009.08.021>
- Karger-Kocsis J, Kmetty Á, Lendvai L et al (2014) Water-assisted production of thermoplastic nanocomposites: a review. *Materials* 8:72–95. <https://doi.org/10.3390/ma8010072>
- Kyrikou I, Briassoulis D (2007) Biodegradation of agricultural plastic films: a critical review. *J Polym Environ* 15:125–150. <https://doi.org/10.1007/s10924-007-0053-8>
- Nocita D, Forte G, Drakopoulos SX et al (2017) Processing and characterization of bio-polyester reactive blends: from thermoplastic blends to cross-linked networks. *Polymer* 132:252–263. <https://doi.org/10.1016/j.polymer.2017.10.069>
- Visco A, Nocita D, Giamporcaro A et al (2017) Effect of Ethyl Ester L-Lysine triisocyanate addition to produce reactive PLA/PCL bio-polyester blends for biomedical applications. *J Mech Behav Biomed Mater* 68:308–317. <https://doi.org/10.1016/j.jmbbm.2017.02.018>
- Loukelis K, Papadogianni D, Chatzinikolaidou M (2022) Kappacarrageenan/chitosan/gelatin scaffolds enriched with potassium chloride for bone tissue engineering. *Int J Biol Macromol* 209:1720–1730. <https://doi.org/10.1016/j.ijbiomac.2022.04.129>
- Loukelis K, Helal ZA, Mikos AG, Chatzinikolaidou M (2023) Nanocomposite bioprinting for tissue Engineering Applications. *Gels* 9:103. <https://doi.org/10.3390/gels9020103>
- Strachota B, Strachota A, Šlouf M et al (2019) Monolithic intercalated PNIPAm/starch hydrogels with very fast and extensive one-way volume and swelling responses to temperature and pH: prospective actuators and drug release systems. *Soft Matter* 15:752–769. <https://doi.org/10.1039/C8SM02153H>
- Peidayesh H, Mosnáčková K, Špitalský Z et al (2021) Thermoplastic starch–based composite reinforced by conductive filler networks: physical properties and electrical conductivity changes

- during cyclic deformation. *Polymers* 13:3819. <https://doi.org/10.3390/polym13213819>
12. Sun T, Zhu C, Xu J (2018) Multiple stimuli-responsive selenium-functionalized biodegradable starch-based hydrogels. *Soft Matter* 14:921–926. <https://doi.org/10.1039/C7SM02137B>
 13. Cyras VP, Manfredi LB, Ton-That M-T, Vázquez A (2008) Physical and mechanical properties of thermoplastic starch/montmorillonite nanocomposite films. *Carbohydr Polym* 73:55–63. <https://doi.org/10.1016/j.carbpol.2007.11.014>
 14. Soykeabkaew N, Thanomsilp C, Suwanton O (2015) A review: starch-based composite foams. *Compos Part A: Appl Sci Manuf* 78:246–263. <https://doi.org/10.1016/j.compositesa.2015.08.014>
 15. Shi R, Liu Q, Ding T et al (2007) Ageing of soft thermoplastic starch with high glycerol content. *J Appl Polym Sci* 103:574–586. <https://doi.org/10.1002/app.25193>
 16. Lendvai L, Karger-Kocsis J, Kmetty Á, Drakopoulos SX (2016) Production and characterization of microfibrillated cellulose-reinforced thermoplastic starch composites. *J Appl Polym Sci* 133:42397. <https://doi.org/10.1002/app.42397>
 17. Lendvai L, Sajó I, Karger-Kocsis J (2019) Effect of Storage Time on the structure and Mechanical Properties of Starch/Bentonite Nanocomposites. *Starch - Stärke* 71:1800123. <https://doi.org/10.1002/star.201800123>
 18. Baran A, Fričová O, Vrabel P et al (2022) Effects of urea and glycerol mixture on morphology and molecular mobility in thermoplastic starch/montmorillonite-type nanofiller composites studied using XRD and NMR. *J Polym Res* 29:257. <https://doi.org/10.1007/s10965-022-03110-6>
 19. Peidayesh H, Heydari A, Mosnáčková K, Chodák I (2021) In situ dual crosslinking strategy to improve the physico-chemical properties of thermoplastic starch. *Carbohydr Polym* 269:118250. <https://doi.org/10.1016/j.carbpol.2021.118250>
 20. Singh T, Gangil B, Patnaik A et al (2019) Agriculture waste reinforced corn starch-based biocomposites: effect of rice husk/walnut shell on physicochemical, biodegradable and thermal properties. *Mater Res Express* 6:045702. <https://doi.org/10.1088/2053-1591/aafe45>
 21. Müller P, Kapin É, Fekete E (2014) Effects of preparation methods on the structure and mechanical properties of wet conditioned starch/montmorillonite nanocomposite films. *Carbohydr Polym* 113:569–576. <https://doi.org/10.1016/j.carbpol.2014.07.054>
 22. van Soest JGG, Vliegthart JFG (1997) Crystallinity in starch plastics: consequences for material properties. *Trends Biotechnol* 15:208–213. [https://doi.org/10.1016/S0167-7799\(97\)01021-4](https://doi.org/10.1016/S0167-7799(97)01021-4)
 23. Avérous L (2004) Biodegradable multiphase systems based on plasticized starch: a review. *J Macromol Sci Part C: Polym Rev* 44:231–274. <https://doi.org/10.1081/MC-200029326>
 24. Majdzadeh-Ardakani K, Navarchian AH, Sadeghi F (2010) Optimization of mechanical properties of thermoplastic starch/clay nanocomposites. *Carbohydr Polym* 79:547–554. <https://doi.org/10.1016/j.carbpol.2009.09.001>
 25. Xie F, Pollet E, Halley PJ, Avérous L (2013) Starch-based nanobiocomposites. *Prog Polym Sci* 38:1590–1628. <https://doi.org/10.1016/j.progpolymsci.2013.05.002>
 26. Lendvai L, Apostolov A, Karger-Kocsis J (2017) Characterization of layered silicate-reinforced blends of thermoplastic starch (TPS) and poly(butylene adipate-co-terephthalate). *Carbohydr Polym* 173:566–572. <https://doi.org/10.1016/j.carbpol.2017.05.100>
 27. Halley PJ, Dorgan JR (2011) Next-generation biopolymers: advanced functionality and improved sustainability. *MRS Bull* 36:687–691. <https://doi.org/10.1557/mrs.2011.180>
 28. Yalpani M (1988) Polysaccharides: syntheses, modifications, and structure/property relations. Elsevier, Amsterdam
 29. Einfeldt J, Meißner D, Kwasniewski A (2001) Polymer dynamics of cellulose and other polysaccharides in solid state-secondary dielectric relaxation processes. *Prog Polym Sci* 26:1419–1472. [https://doi.org/10.1016/S0079-6700\(01\)00020-X](https://doi.org/10.1016/S0079-6700(01)00020-X)
 30. Kremer F, Schönhalz A (2003) Broadband dielectric spectroscopy. Springer, Berlin
 31. Psarras GC (2010) Conductivity and dielectric characterization of polymer nanocomposites. In: Tjong SC, Mai YW (eds) Physical properties and applications of polymer nanocomposites. Elsevier, Amsterdam, pp 31–69
 32. Psarras GC (2018) Fundamentals of dielectric theories. In: Dang ZM (ed) Dielectric polymer materials for high-density energy storage. Elsevier, Amsterdam, pp 11–57
 33. Klonos PA, Terzopoulou Z, Zamboulis A et al (2022) Direct and indirect effects on molecular mobility in renewable polylactide-poly(propylene adipate) block copolymers as studied via dielectric spectroscopy and calorimetry. *Soft Matter* 18:3725–3737. <https://doi.org/10.1039/D2SM00261B>
 34. Šmídová N, Peidayesh H, Baran A et al (2023) Influence of air humidity level on the structure and mechanical properties of thermoplastic starch-montmorillonite nanocomposite during storage. *Materials* 16:900. <https://doi.org/10.3390/ma16030900>
 35. Tsangaris GM, Psarras GC, Kouloumbi N (1998) Electric modulus and interfacial polarization in composite polymeric systems. *J Mater Sci* 33:2027–2037. <https://doi.org/10.1023/A:1004398514901>
 36. Gerhardt R (1994) Impedance and dielectric spectroscopy revisited: distinguishing localized relaxation from long-range conductivity. *J Phys Chem Solids* 55:1491–1506. [https://doi.org/10.1016/0022-3697\(94\)90575-4](https://doi.org/10.1016/0022-3697(94)90575-4)
 37. Drakopoulos SX, Karger-Kocsis J, Kmetty Á et al (2017) Thermoplastic starch modified with microfibrillated cellulose and natural rubber latex: a broadband dielectric spectroscopy study. *Carbohydr Polym* 157:711–718. <https://doi.org/10.1016/j.carbpol.2016.10.036>
 38. Anglès MN, Dufresne A (2000) Plasticized Starch/Tunicin whiskers nanocomposites. 1. *Struct Anal Macromol* 33:8344–8353. <https://doi.org/10.1021/ma0008701>
 39. Drakopoulos SX, Karger-Kocsis J, Psarras GC (2020) The effect of micro-fibrillated cellulose upon the dielectric relaxations and DC conductivity in thermoplastic starch bio-composites. *J Appl Polym Sci* 137:49573. <https://doi.org/10.1002/app.49573>
 40. Havriliak S, Negami S (1967) A complex plane representation of dielectric and mechanical relaxation processes in some polymers. *Polymer* 8:161–210. [https://doi.org/10.1016/0032-3861\(67\)90021-3](https://doi.org/10.1016/0032-3861(67)90021-3)
 41. Drakopoulos SX, Patsidis AC, Psarras GC (2022) Epoxy-based/BaTiO₃ nanodielectrics: relaxation dynamics, charge transport and energy storage. *Mater Res Bull* 145:111537. <https://doi.org/10.1016/j.materresbull.2021.111537>
 42. Johari GP, Goldstein M (1971) Viscous liquids and the glass transition. III. Secondary relaxations in aliphatic alcohols and other nonrigid molecules. *J Chem Phys* 55:4245–4252. <https://doi.org/10.1063/1.1676742>
 43. Schröter K, Donth E (2000) Viscosity and shear response at the dynamic glass transition of glycerol. *J Chem Phys* 113:9101–9108. <https://doi.org/10.1063/1.1319616>
 44. Drakopoulos SX, Karger-Kocsis J, Psarras GC (2019) In situ thermodielectric analysis of the gelatinization mechanism of raw maize starch: an experimental and theoretical approach. *J Polym Environ* 27:333–342. <https://doi.org/10.1007/s10924-018-1348-7>
 45. Mascia L, Kouparitsas Y, Nocita D, Bao X (2020) Antiplasticization of polymer materials: structural aspects and effects on mechanical and diffusion-controlled properties. *Polymers* 12:769. <https://doi.org/10.3390/polym12040769>
 46. Forssell PM, Mikkilä JM, Moates GK, Parker R (1997) Phase and glass transition behaviour of concentrated barley starch-glycerol-water mixtures, a model for thermoplastic starch. *Carbohydr*

- Polym 34:275–282. [https://doi.org/10.1016/S0144-8617\(97\)00133-1](https://doi.org/10.1016/S0144-8617(97)00133-1)
47. Schmitt H, Guidez A, Prashantha K et al (2015) Studies on the effect of storage time and plasticizers on the structural variations in thermoplastic starch. *Carbohydr Polym* 115:364–372. <https://doi.org/10.1016/j.carbpol.2014.09.004>
 48. Adam G, Gibbs JH (1965) On the temperature dependence of cooperative relaxation properties in glass-forming liquids. *J Chem Phys* 43:139–146. <https://doi.org/10.1063/1.1696442>
 49. Berthier L, Biroli G, Bouchaud J-P et al (2005) Direct experimental evidence of a growing length scale accompanying the Glass Transition. *Science* 310:1797–1800. <https://doi.org/10.1126/science.1120714>
 50. Bauer Th, Lunkenheimer P, Loidl A (2013) Cooperativity and the freezing of molecular motion at the glass transition. *Phys Rev Lett* 111:225702. <https://doi.org/10.1103/PhysRevLett.111.225702>
 51. Einfeldt J, Meißner D, Kwasniewski A (2003) Contributions to the molecular origin of the dielectric relaxation processes in polysaccharides – the high temperature range. *J Non-cryst Solids* 320:40–55. [https://doi.org/10.1016/S0022-3093\(03\)00086-3](https://doi.org/10.1016/S0022-3093(03)00086-3)
 52. Karan N, Pradhan D, Thomas R et al (2008) Solid polymer electrolytes based on polyethylene oxide and lithium trifluoromethane sulfonate (PEO–LiCF₃SO₃): ionic conductivity and dielectric relaxation. *Solid State Ionics* 179:689–696. <https://doi.org/10.1016/j.ssi.2008.04.034>
 53. Fragiadakis D, Dou S, Colby RH, Runt J (2008) Molecular mobility, Ion mobility, and mobile ion concentration in poly(ethylene oxide)-based polyurethane ionomers. *Macromolecules* 41:5723–5728. <https://doi.org/10.1021/ma800263b>
 54. Serghei A, Tress M, Sangoro JR, Kremer F (2009) Electrode polarization and charge transport at solid interfaces. *Phys Rev B* 80:184301. <https://doi.org/10.1103/PhysRevB.80.184301>
 55. Yang H, Glynos E, Huang B, Green PF (2013) Out-of-plane Carrier Transport in Conjugated Polymer Thin Films: role of morphology. *J Phys Chem C* 117:9590–9597. <https://doi.org/10.1021/jp402254r>
 56. Angell CA (1997) Why C₁ = 16–17 in the WLF equation is physical—and the fragility of polymers. *Polymer* 38:6261–6266
 57. Wang Y, Fan F, Agapov AL et al (2014) Examination of the fundamental relation between ionic transport and segmental relaxation in polymer electrolytes. *Polymer* 55:4067–4076. <https://doi.org/10.1016/j.polymer.2014.06.085>
 58. Puzenko A, Hayashi Y, Ryabov YE et al (2005) Relaxation dynamics in glycerol – water mixtures: I. glycerol-rich mixtures. *J Phys Chem B* 109:6031–6035. <https://doi.org/10.1021/jp0445122>
 59. Capponi S, Napolitano S, Behrnd NR et al (2010) Structural relaxation in nanometer thin layers of glycerol. *J Phys Chem C* 114:16696–16699. <https://doi.org/10.1021/jp108151p>
 60. Pipertzis A, Papamokos G, Mühlhous M et al (2020) What determines the glass temperature and dc-conductivity in imidazolium-polymerized ionic liquids with a polythiophene backbone? *Macromolecules* 53:3535–3550. <https://doi.org/10.1021/acs.macromol.0c00226>
 61. Namikawa H (1975) Characterization of the diffusion process in oxide glasses based on the correlation between electric conduction and dielectric relaxation. *J Non-cryst Solids* 18:173–195. [https://doi.org/10.1016/0022-3093\(75\)90019-8](https://doi.org/10.1016/0022-3093(75)90019-8)
 62. Dyre JC (1988) The random free-energy barrier model for ac conduction in disordered solids. *J Appl Phys* 64:2456–2468. <https://doi.org/10.1063/1.341681>
 63. Dyre JC, Schröder TB (2000) Universality of ac conduction in disordered solids. *Rev Mod Phys* 72:873–892. <https://doi.org/10.1103/RevModPhys.72.873>
 64. Zardalidis G, Ioannou E, Pispas S, Floudas G (2013) Relating structure, viscoelasticity, and local mobility to Conductivity in PEO/LiTf electrolytes. *Macromolecules* 46:2705–2714. <https://doi.org/10.1021/ma400266w>

Publisher's Note Springer Nature remains neutral with regard to jurisdictional claims in published maps and institutional affiliations.

Springer Nature or its licensor (e.g. a society or other partner) holds exclusive rights to this article under a publishing agreement with the author(s) or other rightsholder(s); author self-archiving of the accepted manuscript version of this article is solely governed by the terms of such publishing agreement and applicable law.

Authors and Affiliations

Stavros X. Drakopoulos^{1,4} · Zdenko Špitalský² · Hamed Peidayesh² · László Lendvai³

✉ Stavros X. Drakopoulos
sd5541@princeton.edu

✉ László Lendvai
lendvai.laszlo@sze.hu

¹ Department of Physics, University of Bath, Claverton Down, Bath BA2 7AY, UK

² Polymer Institute, Slovak Academy of Sciences, Dubravská cesta, 9, 845 41 Bratislava, Slovakia

³ Department of Materials Science and Engineering, Széchenyi István University, Egyetem tér 1, Győr H-9026, Hungary

⁴ Present Address: Department of Chemical and Biological Engineering & Princeton Materials Institute, Princeton University, Princeton, NJ 08544, USA